# Study on main Frequency precursor characteristics of Acoustic Emission from Deep buried Dali Rock explosion

Fuding Mei[1] · Chuanyu Hu[1] · Panyu Li[1] · Junsi Zhang[1]

## Abstract

Rock burst disaster events have become one of the most common disasters in the field of underground engineering, and it is of great practical significance to study the prediction and early warning signs of rock burst. Acoustic emission waveforms generated during a rock burst event, which are often characterized by parameter analysis, that analysis of the waveform spectrum can reflect the characteristics of rock damage and failure. Based on a single-axis strain-type rock burst test of deep buried marble, characteristics of the frequency spectrum, as well as the time-domain dominant frequency of acoustic emissions during the entire rock burst process, were analyzed. We find that the acoustic emission spectrum characteristics also have their own characteristics at different stages of rock burst. In general, The main frequency amplitude value presents an increasing trend, the peak shape of the acoustic emission spectrum shifts between unimodal and multimodal, and the secondary frequency typically appears in the plastic deformation stage. In the high-frequency domain (more than 200 kHz) of the initial loading of stress redistribution, the elastic phase of the energy build-up shows a relatively quiet period, the main frequency distribution of plastic deformation stage shows increasing tendency. Before and after the rock burst event, the dense area of the main frequency migrates from the high-frequency domain to the low-frequency domain, the main frequency in the high frequency field appears dense distribution on the eve of rock burst. These changes were distinguished as characteristic criteria for impending rock burst and can therefore be used for the prediction and early warning of rock burst events.

**Keywords** Rock burst · Marble · Uniaxial loading · Acoustic emission · Spectrum signature

## Introduction

Strain rock burst is a mode of failure in which an energy build-up is rapidly released at the free surface of surrounding rock by man-made excavation (Zhao et al. 2019; Miao et al. 2009; Dehghani and Lohrasb 2019). Strain rock burst is mainly

✉ Chuanyu Hu
chuanhu45@gmail.com; 774185761@qq.com

Fuding Mei
335623206@qq.com

Panyu Li
912227450@qq.com

Junsi Zhang
1026591447@qq.com

[1] China University of Geosciences (Wuhan) Engineering College, Wuhan 430074, Hubei, China

characterized by violent roof collapses and rib spalling of the surrounding rock, and is often accompanied by the ejection of rock fragments and significant noise (Li et al. 2017; Monte 2003). As a result, rock bursts seriously endanger the safety of underground workers and may cause damage to their equipment and facilities.

Acoustic emission (AE), also known as stress wave emission, is a phenomenon in which an external load causes local internal damage to a material, and the energy build-up is rapidly released in the form of elastic waves (Pieri et al. 2001; Tan Chee & Mba, 2005; Kasai and Utatsu 2009; Yang et al. 2009; Liu and Xu 2013). It was discovered that the AE phenomenon is generated by rock-type materials under external loads; the AE technique has been widely used for studying rock instability and failure (Yuan et al. 1985). AE parameters and waveform characteristics are often used for analysis in laboratory simulations of rock burst. AE parameter characteristics mainly include event count, ringing count, amplitude, energy count, and RMS voltage. In waveform analysis, the frequency and amplitude of the AE spectrum of the test process is studied to qualitatively assess the stability of the rock during the loading

process. Compared to the parametric analysis method in the time domain, the waveform analysis method in the frequency domain better reflects the intrinsic information of the internal rupture source of the rock (He et al. 2015).

In the uniaxial compression AE test, Chen found that the frequency spectrum showed little change in the initial stage of stress loading but changed suddenly when the stress reached the failure limit, at which time the shape of the spectrum also changed from a single peak to multiple peaks (Chen 1990). Pan et al. exerted uniaxial loading on rock with a rock burst tendency using an electro-hydraulic servo rigidity testing machine; the results showed that as the stress increased, the AE spectrum evolved from low-frequency to high-frequency, and the front edge of the AE waveform became steep near the peak load (Pan et al. 2001).

Jiang et al. established the relationship between AE parameters and the failure mechanism of salt rock through uniaxial compression tests of salt rock under different loading strain rates (Jiang et al. 2012). The tests revealed the evolution of damage of salt rock under different strain rates. Specifically, the faster the loading rate, the higher the AE frequency, and the more significant the brittle failure characteristics (Zhao et al. 2018).

Zhao et al. used the indoor MTTA true triaxial rock burst simulation test system to extract AE characteristic waveforms of various stages in the granite rock burst process for fast Fourier transform (FFT) (Zhao et al. 2019). They found that the dominant frequency of AE in the test process presented an overall trend of shifting from low frequency to high frequency and back to low frequency. Furthermore, they found that the dominant frequency concentrated in the low-frequency range of 90 to 120 kHz could be used as a characteristic frequency to predict the rock burst of granite. Su et al. used a true triaxial rock burst test machine to simulate the granite rock burst process (Guoshao et al. 2016). Their study showed that there was a "relatively quiet period" of the AE waveform signal, which had a small amplitude when it was close to rock burst ejection failure. During the test, the dominant frequency of AE showed a trend of migrating from high frequency to low frequency, and the shape of the frequency spectra alternated between multiple peaks and a single peak (Azadi et al. 2019; Liu et al. 2019).

In this study, the uniaxial compression AE test was conducted to investigate the dominant frequency characteristics of AE throughout the entire rock burst process. Briefly, the original waveforms of AE at critical moments of rock burst were extracted, and the FFT was used to obtain the frequency-domain information of AE at the critical moments. The dominant frequency information of all original AE waveforms was extracted using MATLAB and the time-domain characteristics of the AE dominant frequency were analyzed. Finally, the intrinsic information of AE waveforms for different stages of rock burst were investigated through analysis of the frequency-domain and time-domain evolution trends of the original AE waveforms of the rock burst test. As a result, the correlation between the AE waveform characteristics of the entire rock burst process and the intensity of the rock burst were determined, thereby providing a theoretical basis for identifying early warning signs and predicting rock burst events in real-time.

## Rock burst test

### Rock specimen

A marble core was collected from the middle of an 810-m section of the Daye Tonglushan Copper-iron Mine (Fig. 1a). The deformation rate analysis (DRA) method showed that the middle section of the marble core had an average geostatic stress of 26.26 MPa, indicating a provenance of deep burial and high ground-stress (Chen et al. 2015), which are conditions favorable for occasional rock bursts. According to the Standard for Test Methods of Engineering Rock Mass (GB/T50266-2013), standard specimens with dimensions of 50 mm × 100 mm were prepared (Fig. 1b). The specimens had a grayish white appearance and contained a small number of ore spots. The whole rock was relatively dense and massive, with no significant cracks. X-ray dust diffraction experiments showed that the main mineral composition of the marble core was calcite, along with a small amount of secondary clay minerals such as mica.

### Test methods

The rock burst test device consisted of the RMT-150C multifunctional rock experimental system (Wuhan Geotechnical Engineering Institute) and the PCI-II type system [Physical Acoustics Corporation (PAC), USA], as shown in Fig. 2a. The former has a maximum vertical output of 1000 kN, a loading rate of 0.01 to 100 kN/s, and a deformation rate of 0.0001–1.0 mm/s, while the latter has a maximum sampling frequency of 40 MHz, an 18-digit digital-to-analog conversion capability, and the ability to record various characteristic parameters such as ringing count, energy, and amplitude, as well as complete waveforms of AE.

The AE sensor was fixed to the side of the test specimen with insulating tape, and Vaseline was evenly applied on the contact surface to ensure good coupling (Fig. 2b). The loading system adopted displacement control with a loading rate of 0.0010 mm/s. The AE sampling frequency was set to 1 M/s, and the gain was set to 45 dB. The AE monitoring system and the loading system were started synchronously, and the experiment was stopped when the overall specimen became unstable and ruptured.

Fig. 1  Rock specimens. **a** Field cores. **b** Specimens

## Test results

It was observed that the significant rock burst occurred in the rock specimen both near and during the instability failure stage (Mo 2015; He et al. 2007; Zhang et al. 2016). Additionally, these studies indicated that rock burst can be analyzed from acoustic duration, rock surface dynamic failure, failure surface characteristics, and penetrating cracks. In the present study, two groups of marble specimens labeled N5 and N7 were investigated, and their rock burst phenomena and failure surface characteristics were analyzed.

In the initial stage of loading, specimen N5 underwent a short stage of compaction, during which a slight friction sound emitted and the surface of the specimen remained intact. Subsequently, the specimen entered an elastic stage but showed no significant changes. When the specimen was loaded for 392 s and the stress was near the peak load of 79 MPa, the surface of the rock specimen showed slight rock fragmentation and spalling, and rock dust slipped from the spalling area with a slight bursting sound, demonstrating that the specimen was in the initial stage of rock burst. As the load continued to increase, rock fragments mixed with rock dust were ejected from the surface of the specimen with a continuous bursting sound, and visible cracks appeared on the specimen's surface. As loading continued for a total 515 s, rock fragments were ejected with a loud bursting sound, macro-cracks were formed on the surface of the specimen, multiple cracks coalesced with each other, pieces of rock began to collapse, and the specimen experienced violent rock burst. It took 123 s from the initial stage of minor rock burst to the late stage of violent rock burst, and the axial stress decreased to 60 MPa (Fig. 3). From the morphology of the final failure surface (Fig. 4), we observed that the specimen had a typical V-shaped rock burst pit with a stepped, zig-zagged surface, Y-shaped shear cracks penetrated the rock and five large rock pieces had spalled, some rock dust was transferred to the testbed (indicating that specimen N5 underwent a relatively violent rock burst), penetrating cracks appeared, and the whole rock mass became unstable. Overall, the damage to the rock was significant; it exhibited both a V-shaped rock burst pit and penetrating shear cracks.
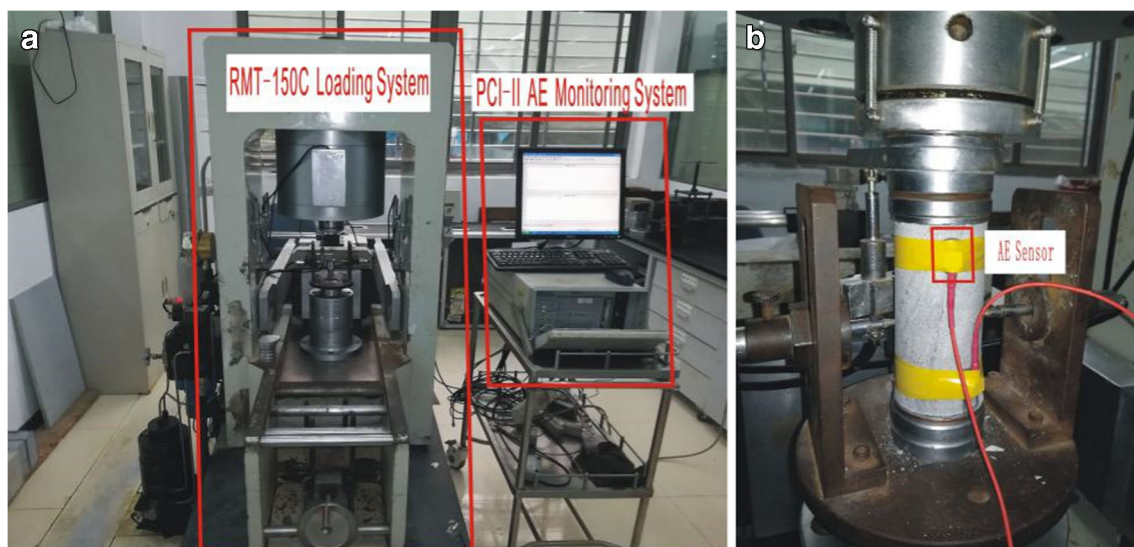


Fig. 2  Test equipment and specimen. **a** Experimental equipment. **b** Specimen

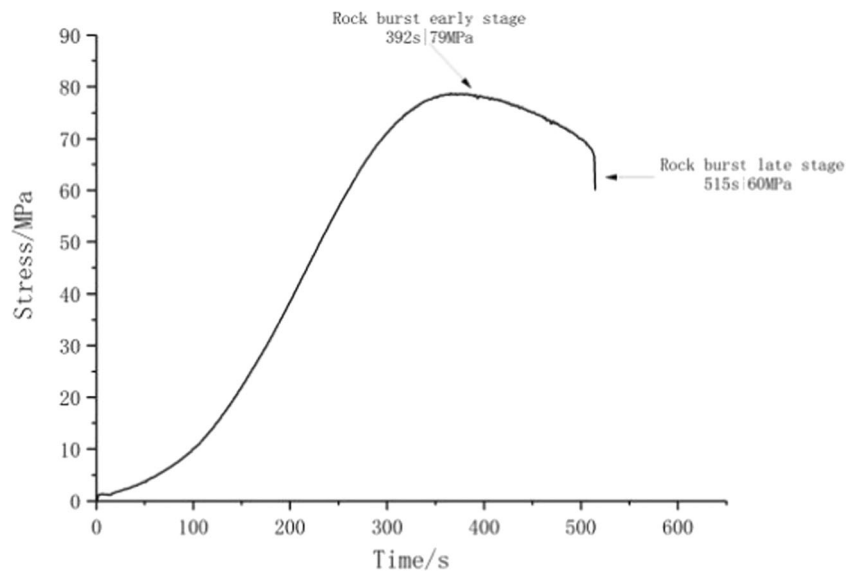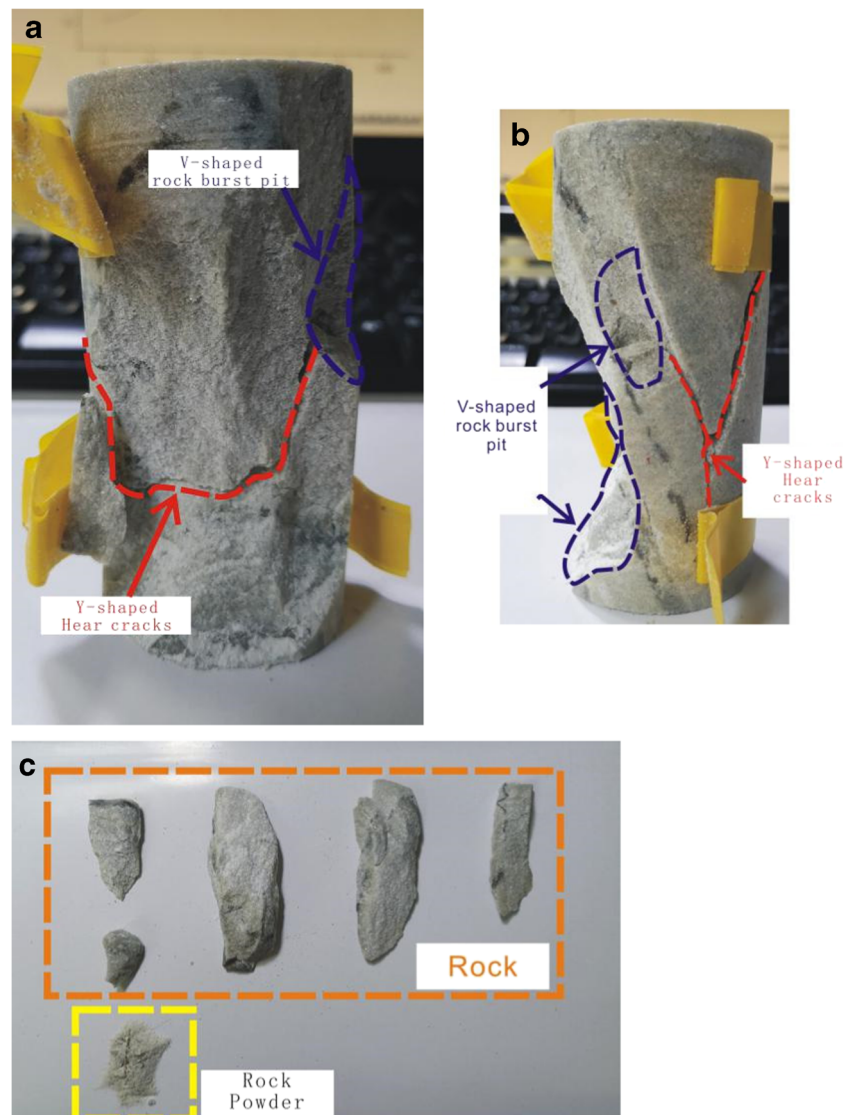**Fig. 3** Time-stress curve of specimen N5



**Fig. 4** Final failure mode of specimen N5. **a** Front view. **b** Side view. **c** Rock fragments

At the initial stage of loading, the characteristics of specimen N7 were similar to those of specimen N5. There was a slight friction sound and no significant crack development was observed on the surface of the specimen. After the specimen was loaded for 377 s, when the stress was near the peak load of 73 MPa, rock fragments collapsed, a small amount of rock dust was ejected, and visible cracks appeared on the side of the specimen accompanied by a loud bursting sound. As the axial stress continued to increase, macro-cracks appeared on the surface of the specimen, cracks coalesced with each other, and rock fragments were ejected from the surface of the rock mass that were accompanied by a loud bursting sound. Finally, the rock mass collapsed. Eight seconds elapsed from the initial stage of rock burst to the late stage of rock burst (Fig. 5), during which the specimen exhibited increasingly severe symptoms of rock burst. The morphology of the final failure surface of specimen N7 (Fig. 6) revealed that there was no significant V-shaped rock burst pit, but there were many shear cracks and splitting cracks. Additionally, the rock fragments were large and the entire rock spalled, indicating that specimen N7 underwent violent rock burst with a short duration of overall instability and failure as well as a dramatic rate of energy release.

## Frequency spectral characteristics of full time-domain AE of rock burst

### Frequency spectral characteristics of AE at critical moments of rock burst

AE spectral analysis is a commonly used method in AE waveform analysis. The method interprets the signal of an AE waveform by mapping it from the time domain to the frequency domain. Furthermore, spectral analysis is effective in reflecting the dynamic rupture and damage characteristics of the AE source (Xu et al. 2014; Jia 2013). The AE signal generated during the rock damage process under loading is a discrete non-stationary signal, and the original AE waveform signal can be extracted by a classical spectrum analysis method, FFT (Nobukatsu 2002), to obtain the two-dimensional AE spectrum at the critical moments of the rock burst test. Jia defined the dominant frequency as the frequency corresponding to the maximum amplitude in the two-dimensional spectrum (Jia 2013; Xu et al. 2019). Previous experimental results showed that the dominant frequency as well as the secondary dominant frequency, which corresponds to the peak shape with an amplitude lower than that of the dominant frequency but significantly higher than that of other frequency bands, appear in the rock rupture process (Zhang et al. 2019; Zhang et al. 2014; Li et al. 2010; Shen et al. 2019).

In this study, critical moments were selected from each stage of the rock burst test (i.e., compaction stage, linear elastic stage, plastic deformation stage, near rock burst stage, initial stage of rock burst, and late stage of rock burst) and used as objects in two-dimensional AE spectral analysis. According to the experimental phenomena and referring to the entire stress-strain curve, six critical moments were selected and the acoustic waveforms were extracted according to these moments. FFT was performed using MATLAB to obtain the two-dimensional AE spectra at each different critical moment. Using the above method, the two-dimensional AE spectra of specimens N5 and N7 at six critical moments were obtained, as shown in Figs. 7 and 8, respectively.

As shown in Fig. 7, in the compaction stage of N5 (19 s), the frequency of the dominant frequency was 273.4 kHz and
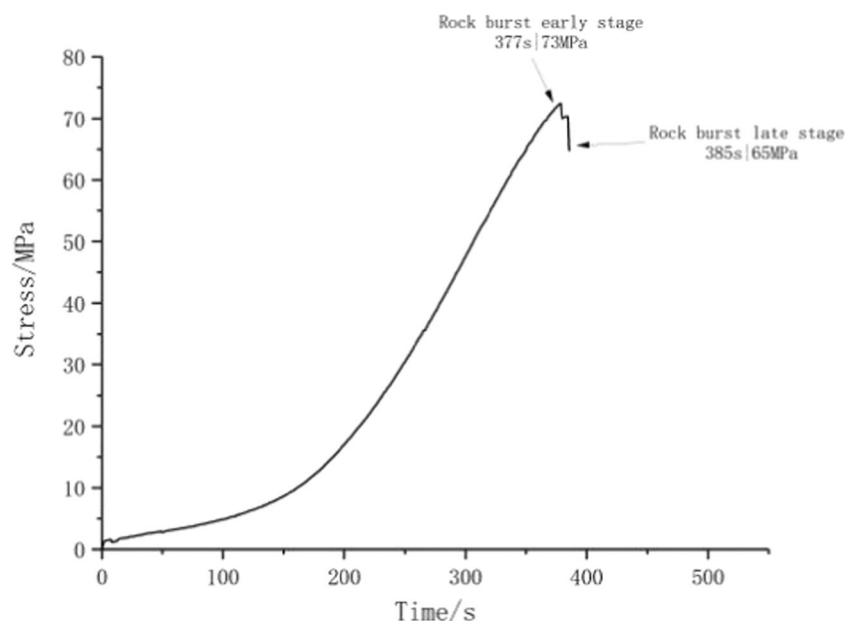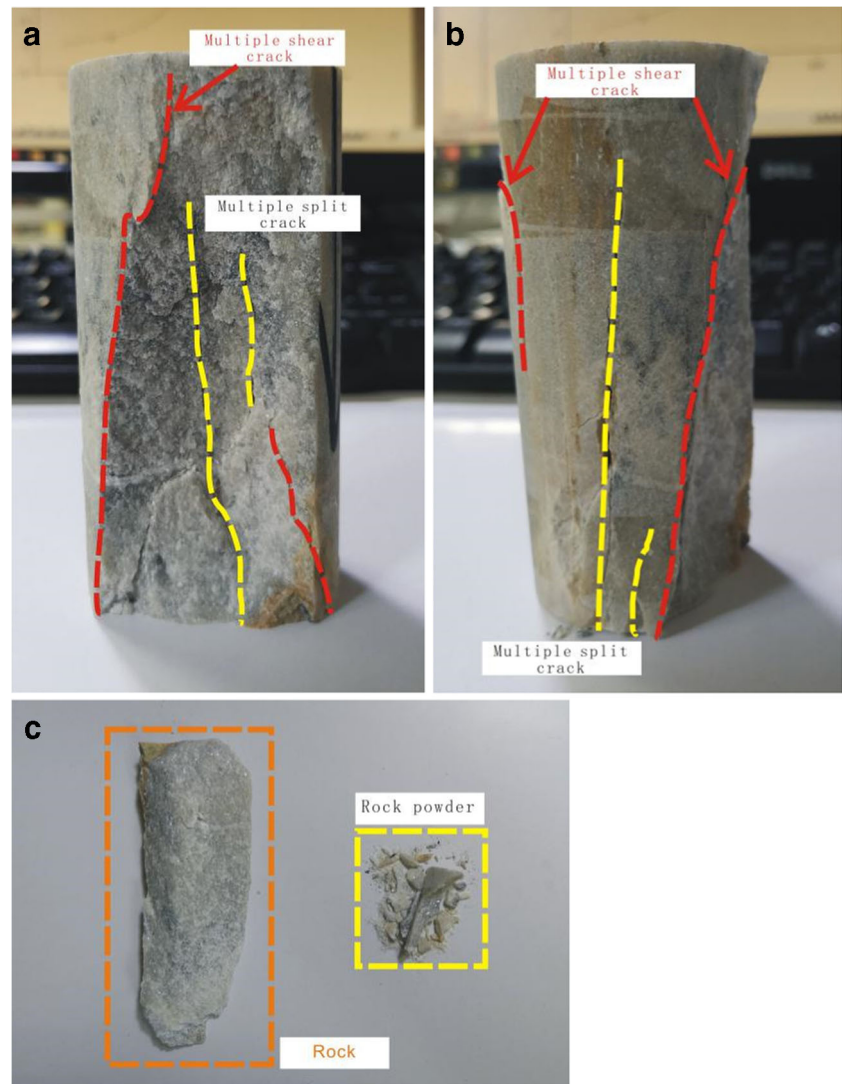
**Fig. 5** Time-stress curve of specimen N7

**Fig. 6** Final failure mode of
specimen N7. **a** Front view. **b**
Side view. **c** Rock fragments



the maximum amplitude was 4.194 mV. In the linear elastic
stage (71 s), the dominant frequency decreased to 19.53 kHz
and the amplitude showed an increasing trend, reaching
10.5 mV; however, the frequency band narrowed. In the plas-
tic deformation stage (250 s), the dominant frequency and
amplitude increased to 244.1 kHz and 17.3 mV, respectively,
and, at the same time, the secondary frequency appeared with
a relatively low-frequency of 9.766 kHz. The frequency band
became wider during the plastic deformation stage (250 s). In
the near rock burst stage (355 s), the frequency of the domi-
nant frequency increased to 302.7 kHz, the amplitude in-
creased to 20.05 mV, the secondary frequency continued to
exist with a frequency of 19.53 kHz, and the frequency band
became wider. In the early stage of rock burst (392 s), the
frequency of the dominant frequency decreased to
283.2 kHz, the amplitude continued to increase to 22.99 mV,
the secondary frequency continued to exist, and the frequency
band was relatively wide. In the late stage of rock burst
(515 s), the frequency of the dominant frequency decreased

to 29.3 kHz, the secondary frequency disappeared, and the
frequency band narrowed. In contrast, the amplitude reached
a maximum value of 56.01 mV.

As shown in Fig. 8, during the compaction stage of N7
(20 s), the frequency of the dominant frequency was
283.2 kHz and the maximum amplitude was 4.681 mV.
In the linear elastic stage (226 s), the frequency decreased
to 19.53 kHz while the amplitude increased to 10.57 mV;
the frequency band narrowed during this stage. In the plas-
tic deformation stage (350 s), the frequency of the domi-
nant frequency increased to 253.9 kHz, the amplitude de-
creased to 3.384 mV, the secondary frequency occurred at a
relatively low-frequency of 9.766 kHz, and the frequency
band started to widen. In the near rock burst stage (375 s),
the frequency of the dominant frequency and the amplitude
increased to 263.7 kHz and 11.22 mV, respectively, where-
as the secondary frequency remained at 29.3 kHz and the
frequency band became narrower. In the initial stage of
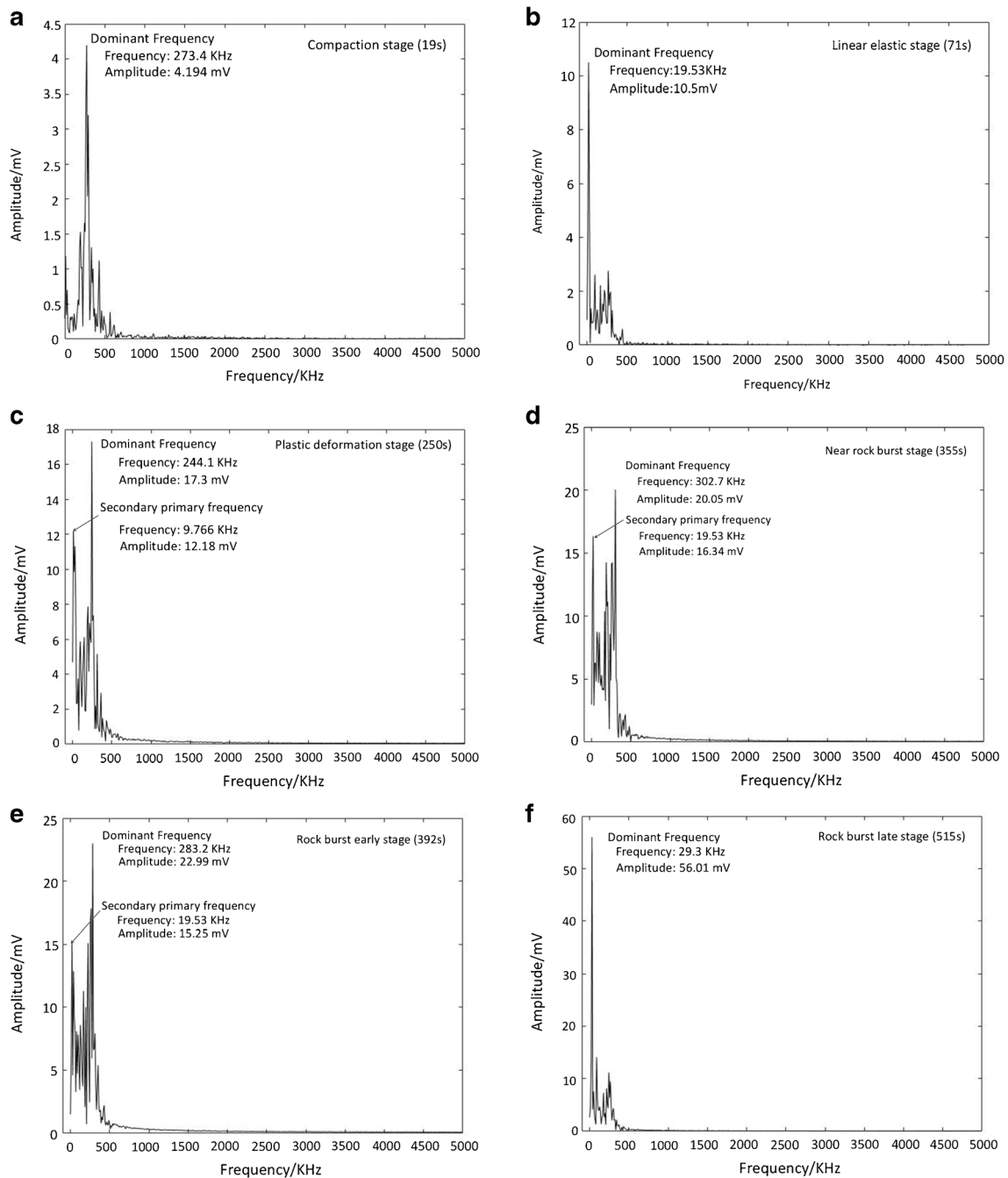rock burst (377 s), the frequency of the dominant

**Fig. 7** AE spectra of different critical stages of specimen N5. **a** Compaction stage. **b** Linear elastic stage. **c** Plastic deformation stage. **d** Near rock burst. **e** Initial stage of rock burst. **f** Late stage of rock burst

frequency remained at 263.7 kHz and the amplitude continued to increase to 18.61 mV; the secondary frequency and bandwidth did not change. In the late stage of rock burst (385 s), the frequency of the dominant frequency and the amplitude decreased to 19.53 kHz and 3.217 mV, respectively. The secondary frequency remained stable at 273.4 kHz, which was greater than the dominant frequency, and the frequency band was widened.

The above analysis showed that the frequency of the dominant frequency exhibited a variable pattern. The high-frequency components revealed the activity intensity of micropores in the rock. Initial increases in values reflected the closure of pores inside the rock, and the continued trend indicated the formation and development of pores in the rock. The low-frequency components revealed that the rock remained stable or had large macro-cracks. The amplitude of the dominant frequency showed an
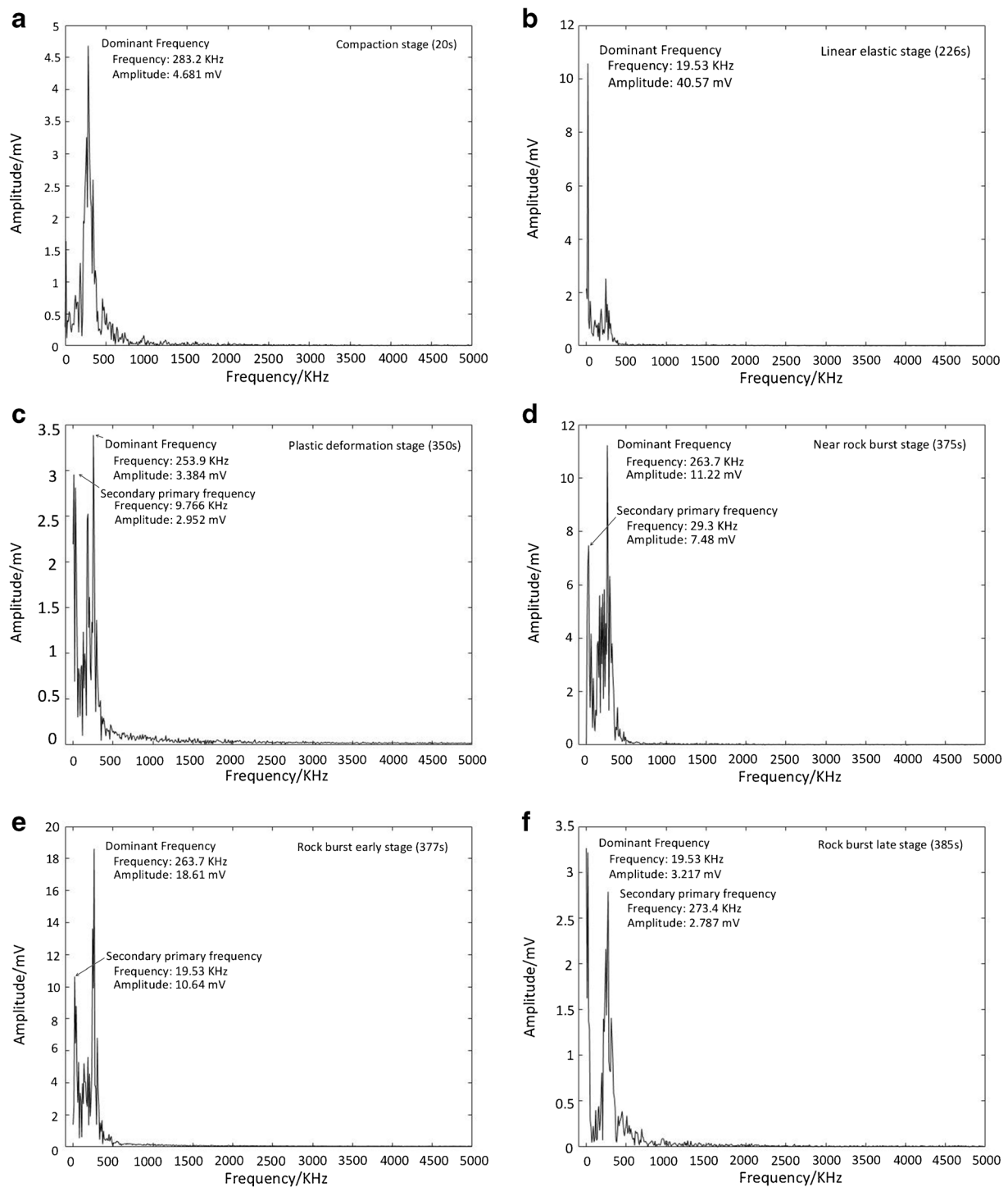
**Fig. 8** AE spectra of different critical stages of specimen N7. **a** Compaction stage. **b** Linear elastic stage. **c** Plastic deformation stage. **d** Near rock burst. **e** Initial stage of rock burst. **f** Late stage of rock burst

overall increasing trend, indicating that the pores and crack propagation in the rock were intensified. The peak shape of the AE frequency spectrum showed a shift from a single peak to multiple peaks, and the secondary frequency often appeared for the first time in the plastic deformation stage, suggesting that the appearance of the secondary frequency indicates irreversible damage to the rock under an external load.

## Full time-domain dominant frequency characteristics of AE of rock burst

FFT was performed for all original AE waveform data for the entire rock burst process of specimens N5 and N7, including a total of 4222 and 11,275 original waveform files, respectively. Each file was collected for 1 ms and was composed of 1024

values. The dominant frequencies of all waveform files after FFT were extracted by MATLAB, and the scatter plot and scatter density plot of the full time-domain dominant frequency characteristics of AE of the rock burst process were drawn according to the AE wave hit sequence, as shown in Figs. 9 and 10, respectively.

In Figs. 9 and 10, the two red lines parallel to the vertical axes indicate the initial and late stages of rock burst, respectively. In each of the two figures, panel a is the scatter distribution of the full time-domain dominant frequency characteristics of the AE of rock burst, and panel b is the corresponding scatter density plot. The color shading represents the density of the dominant frequency distribution of the area; the darker the color, the more concentrated the dominant frequency.

Analysis of Figs. 9 and 10 reveals two patterns of change in the frequency of the dominant frequency. First, the dense area of the dominant frequency of the low-frequency domain (lower than 50 kHz) migrated from the 9.766 kHz frequency band to the 19.53 kHz frequency band. Second, the high-frequency domain (higher than 200 kHz) was densely distributed for the first time in the compaction stage at initial loading, occasionally occurred in the linear elastic stage of energy build-up, began to increase in the plastic deformation stage when irreversible damage to the rock occurred, and appeared densely before and after the rock burst event. Therefore, the migration of the dense area of the dominant frequency in the low-frequency domain to a higher frequency, as well as the density of the dominant frequency distribution in the high-frequency domain, can be used as characteristic criteria for the prediction of rock burst.

Analysis of Figs. 9 and 10 also reveals an interesting phenomenon. That is, a large number of AE wave signals were triggered in the compaction and linear elastic stages, whereas a relatively small number of AE wave signals were triggered in the plastic deformation stage and the stages before and after the rock burst occurred. The reason for this phenomenon may be that the closure of the pores in the rock released many low-frequency low-energy stress waves, thereby triggering a large number of AE signals. Comparatively, a small number of high-frequency high-energy stress waves were released during the formation and development of pores and cracks in the rock.

## Conclusions

(1) In the early stage of loading on the rock specimen, there were no significant results. In the early stage of rock burst, however, there was slight fragmentation and spalling at the rock surface, and rock dust was removed from the spalling area with a slight bursting sound. As the stress increased, rock fragments mixed with rock dust were ejected from the surface of the specimen with a continuous bursting sound, and visible cracks appeared on the surface of the specimen. In the later stage of rock burst, rock fragments were ejected, accompanied by a loud bursting sound, macro-cracks formed on the surface of the specimen, multiple cracks coalesced with each other, rock fragments began to collapse, and the specimen experienced violent rock burst.
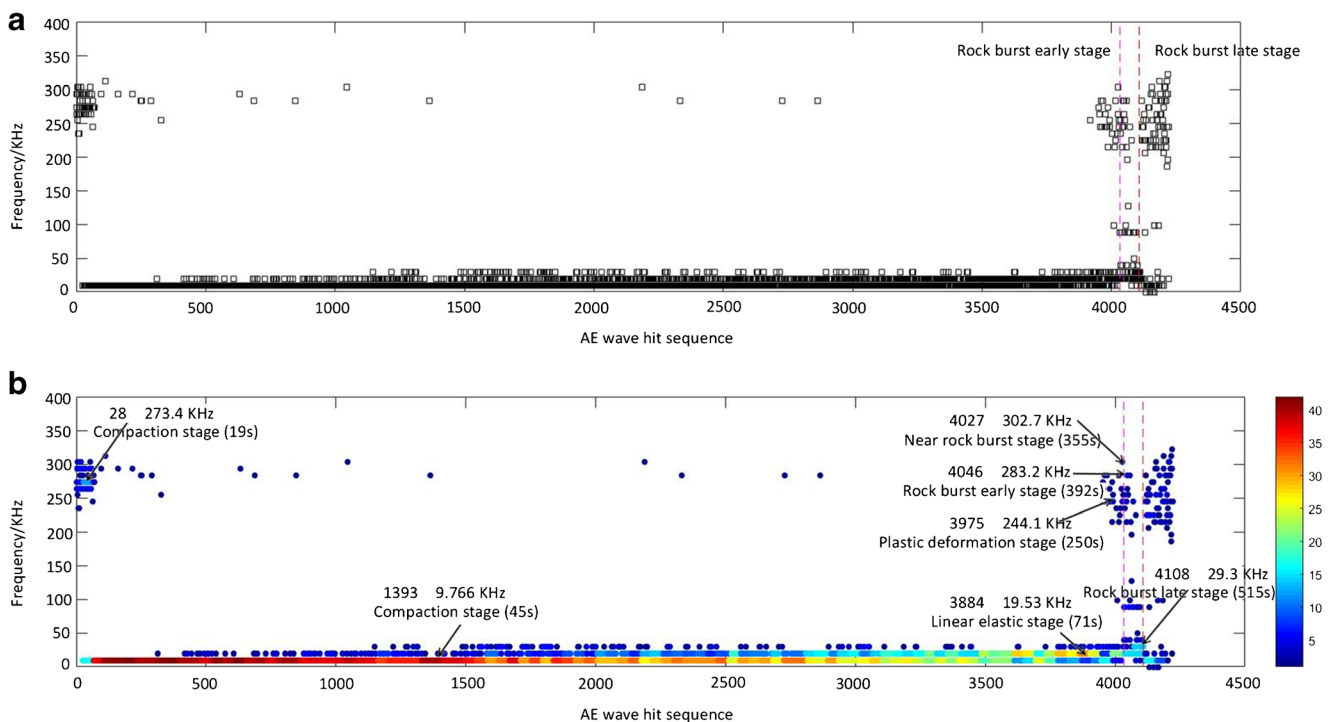


Fig. 9 Scatter plot of full time-domain dominant frequency characteristics of AE of rock burst in specimen N5
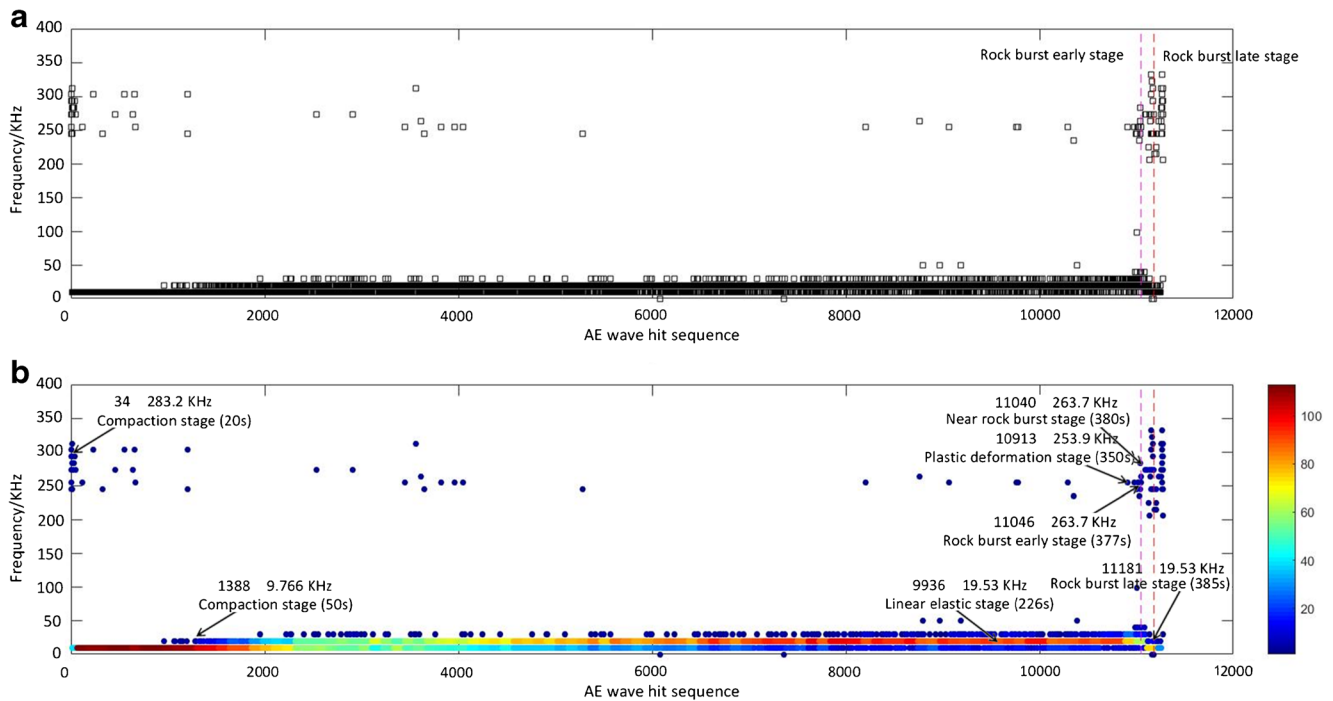
Page 10 of 11Arab J Geosci (2019) 12: 645



Fig. 10 Scatter plot of full time-domain dominant frequency characteristics of AE of rock burst in specimen N7

(2) Based on analysis of AE spectral characteristics at six critical moments during the entire rock burst process, it was found that the frequency of the dominant frequency was variable. The high-frequency components reflected the activity intensity of micropores in the rock, whereas the low-frequency components indicated that the rock remained relatively stable or had large macro-cracks. The amplitude of the dominant frequency showed an overall increasing trend, indicating that the pores and crack propagation became intensified during the rock burst process. The peak shape of the AE spectrum showed a transition from a single peak to multiple peaks, and the secondary frequency appeared during the plastic deformation stage. The appearance of the secondary frequency indicates irreversible damage to the rock under an external load.

(3) Analysis of the scatter plot and scatter density plot of the full time-domain dominant frequency characteristics of the AE of rock burst, we found that the dense area of the dominant frequency of the low-frequency domain (lower than 50 kHz) migrated from the 9.766 kHz frequency band to the 19.53 kHz frequency band. The high-frequency domain (higher than 200 kHz) was densely distributed in the initial stage of loading and showed a "relatively quiet period" in the linear elastic stage of energy build-up. Following these stages, the high-frequency domain began to increase during the plastic deformation stage and was densely distributed before and after rock burst. Therefore, the migration of the dense area of dominant frequency from the low-frequency domain to the high-frequency domain, as well as the variation in density of the dominant frequency distribution of the high-frequency domain, can serve as characteristic criteria for the prediction and early warning of marble rock burst.

## References

Azadi M, Sayar H, Ahmad G-G, Jafari SM (2019) Tensile loading rate effect on mechanical properties and failure mechanisms in open-hole carbon fiber reinforced polymer composites by acoustic emission approach. Compos Part B 158:448–458

Chen D (1990) Frequency and acoustic emission characteristics of sandstone under uniaxial compression [Z]. Science Press, Xiangtan, p 1990

Chen F, He C, Deng J (2015) Concept of high geostress and its qualitative and quantitative definitions. Rock Soil Mech 4:971–980

Dehghani B, Lohrasb F (2019) Experimental investigations of fracture toughness and crack initiation in marble under different freezing and thermal cyclic loading. Constr Build Mater 220:340–352

Guoshao S, Yanjiong S, Xiating F et al (2016) Acoustic signal characteristics in rockburst process. Chin J Rock Mech Eng 6:1190–1201

He M, Miao J, Li D et al (2007) Experimental study on rockburst processes of granite specimen at great depth. Chin J Rock Mech Eng 05:865–876

He M, Zhao F, Zhang Y et al (2015) Feature evolution of dominant frequency components in acoustic emissions of instantaneous strain-type granitic rockburst simulation tests. Rock Soil Mech 01: 1–8

Springer

Jia X (2013) Intrinsic spectral characteristics of acoustic emission of strain rockburst test [D]. China University of Mining and Technology, Beijing, p 2013

Jiang D, Jie C, Song R et al (2012) Experimental study of strain rate effect and acoustic emission characteristics of salt rock under uniaxial compression. Chin J Rock Mech Eng 02:326–336

Kasai N, Utatsu K (2009) Correlation between corrosion rate and AE signal in an acidic environment for mild steel. Corros Sci 8(51):1679

Li N, Wang E, Zhao E et al (2010) Experiment on acoustic emission of rock damage and fracture under cyclic loading and multi-stage loading. J China Coal Soc 35(07):1099–1103

Li D, Zhu Q, Zilong Z, Xibing L, Ranjith PG (2017) Fracture analysis of marble specimens with a hole under uniaxial compression by digital image correlation. Eng Fract Mech 183:109–124

Liu S, Xu J (2013) Study on dynamic characteristics of marble under impact loading and high temperature. Int J Rock Mech Min Sci 62:51–58

Liu S, Li X, Li Z, Chen P, Yang X, Liu Y (2019) Energy distribution and fractal characterization of acoustic emission (AE) during coal deformation and fracturing. Measurement 136:122–131

Miao J, He M, Li D et al (2009) Acoustic emission characteristics of granite under strain rockburst test and its micro-fracture mechanism. Chin J Rock Mech Eng 08:1593–1603

Mo C (2015) Experimental study on the rockburst failure process of the hard rock mass [D]. Guangxi University, p 2015

Monte M (2003) Oxalate film formation on marble specimens caused by fungus. J Cult Herit 4(3):255–258

Nobukatsu TYM (2002) Digital watermarking by a holographic technique. Appl Opt 5(41):865–873

Pan C, Zhu F, Cao P et al (2001) Characteristics of acoustic emission of bursting-intended rocks under uniaxial compression, vol 04. Journal of central south university of technology, pp 336–338

Pieri M, Burlini L, Kunze K, Stretton I, Olgaard DL (2001) Rheological and microstructural evolution of Carrara marble with high shear strain: results from high temperature torsion experiments. J Struct Geol 23(9):1393–1413

Shen R, Qiu L, Zhao E, Han X, Li H, Hou Z, Zhang X (2019) Experimental study on frequency and amplitude characteristics of acoustic emission during the fracturing process of coal under the action of water. Saf Sci 117:320–329

Tan Chee K, Mba D (2005) Identification of the acoustic emission source during a comparative study on diagnosis of a spur gearbox. Tribol Int 38(5):469–480. https://doi.org/10.1016/j.triboint.2004.10.007

Xu Z, Li G, Dong T et al (2014) Overview on development of acoustic emission signal analysis technique and processing. Mater Rev 9:56–60

Xu D, Liu PF, Li JG, Chen ZP (2019) Damage mode identification of adhesive composite joints under hygrothermal environment using acoustic emission and machine learning. Compos Struct 211:351–363

Yang SQ, Dai YH, Han LJ, Jin ZQ (2009) Experimental study on mechanical behavior of brittle marble samples containing different flaws under uniaxial compression. Eng Fract Mech 76(12):1833–1845

Yuan Z, Ma Y, He Z (1985) Acoustic emission technique and its applications [M]. China Machine Press, Beijing

Zhang N, Qi Q, Ouyang Z et al (2014) Experimental on acoustic emission characteristics of marble with different stress paths. J China Coal Soc 39(02):389–394

Zhang Y, Peng L, Xiangxin L et al (2016) An experimental study of predicting rockburst in granitic roadway based on multiparameter normalization. Rock Soil Mech 01:96–104

Zhang Y, Liang P, Sun L et al (2019) Experimental study on acoustic emission spectrum characteristics of saturated granite under uniaxial compression. Rock Soil Mech 40(7):1–11

Zhao J, Feng XT, Zhang X, Yang C, Zhou Y (2018) Time-dependent behaviour and modeling of Jinping marble under true triaxial compression. Int J Rock Mech Min Sci 110:218–230

Zhao F, He M, Wang H et al (2019) Acoustic emission characteristics of granite with different heights under rockburst tests. Rock Soil Mech 01:1–13